# Measurement and Simulation of Low Carbon Steel Alloy Deposit Temperature in plasma Arc Welding Additive Manufacturing

***Abdullah Alhuzaim***

*Jubail Technical Institute, Jubail Industrial City, 31961, Saudi Arabia*
*Alhuzaim_af@jti.edu.sa, +966-50433-4699*

***R. Bruce Madigan***

*Montana Tech of The University of Montana, Butte, MT 59701 USA bmadigan@mtech.edu, +1406-496-4576*

## Abstract

*Additive manufacturing has the potential to produce near-net shape parts directly from weld metal. Prior work has proved that it is possible to directly manufacture components with complex geometric features and with good productivity. However, under high productivity conditions, deposit temperature increases to a level that it is no longer possible to develop appropriate deposit microstructure and therefore mechanical properties. In this study, Plasma Arc welding was used to produce experimental deposits of 1018 low carbon steel under various conditions. An analytical heat flow model was developed to study the influence of interlayer wait time on deposit temperature and therefore grain size and hardness. The results of the model indicated that as wall height increased, the rate of deposit heat removal by conduction to the substrate decreased leading to a higher preheat temperature after a fixed interlayer wait time causing grain size to increase as wall height increased. However, the model results also show that as wall height increased, the deposit surface area from which heat energy is lost via convection and radiation increased. The model also demonstrated that the use of a means of forced convection to rapidly remove heat from the deposit could be an effective way to boost productivity and maintain smaller grain size and therefore higher hardness and strength in the deposit.*

**Keywords:** Additive Manufacturing, Direct Manufacturing, Free from Fabrication, Metal Deposit, Plasma Arc Welding, Shot Form Feedstock Delivery.

## Introduction

The concept of directly manufacturing a component completely out of weld metal has been a possibility for nearly 25 years (Ref.1,2). Additive manufacturing offers the potential to save significant amounts of energy and resources (Ref.3,4) and overcome some limitations of traditional manufacturing methods such as casting, forging and machining. The use of the Plasma Arc welding process for additive manufacturing promises to produce low cost products from vitally important metal alloys (Ref.5). Previous work has demonstrated that it possible to produce relatively complex part shapes and that it is possible to boost metal deposition rate to increase productivity (Ref.6). Attention is now being turned to attaining acceptable mechanical properties and fine geometric features in additively manufactured deposits (Ref.7,8). While the general processing parameters required to produce certain microstructures and hence mechanical properties in low carbon steel alloys are well known, it is difficult to achieve both high productivity and acceptable mechanical properties simultaneously in additively-manufactured. A significant amount of work is being conducted to characterize additive manufacturing process parameters for different alloys. Fusion welding processes like electron beam welding, laser welding, plasma arc welding and gas tungsten arc welding subject the additively manufactured deposit to

repetitive and cumulative thermal cycles that cause complex transformations in steel alloys. The work presented here begins to focus on the next important next step for the PAW process: deposit thermal management to control deposit temperature and therefore microstructure development and resulting mechanical properties.

## Investigation Overview

Experimental PAW deposits of alloy 1018 were made under various conditions. A simple analytical heat flow model was developed to simulate the deposit build process. The model was tuned using experimental data in order to extrapolate and predict deposit temperature over a range of conditions that would be cost prohibitive to investigate experimentally. The influence of a limited range of experimental processing conditions on microstructure development was revealed by metallographic observations. The results of the model form the basis on which to develop a strategy to manage deposit heat flow in order to simultaneously improve productivity and obtain acceptable microstructure and mechanical properties.

## Experimental Deposit Build Procedure

Linear wall deposits were built on a substrate via Plasma Arc Welding (PAW) with steel shots (Fig. 1). Both the substrate and shots was Alloy 1018.
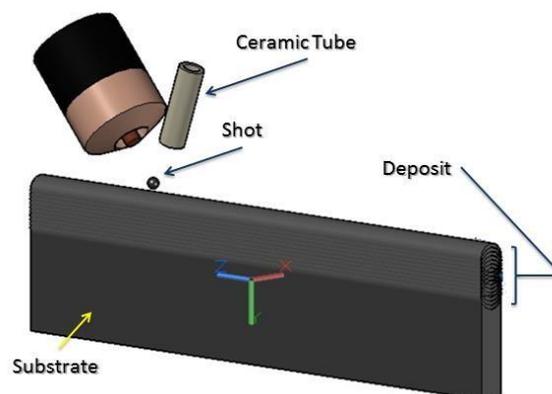


*Figure 1: shows the positioning of the PAW torch and shot delivery tube above the substrate  prior to welding*

The substrate was clamped to a positioning fixture within the Robot the substrate was fixed on the positioner, and the torch standoff distance was set by adjusting the arm torch positioner. The various essential PAW parameters were then set and are shown in the Results and Discussion section for each wall specimen. The essential PAW parameter ranges used to manufacture the weld metal specimens for the additive manufacturing processes are given in Table 1 (Fig. 2). Welding parameters are detailed in Appendix A.
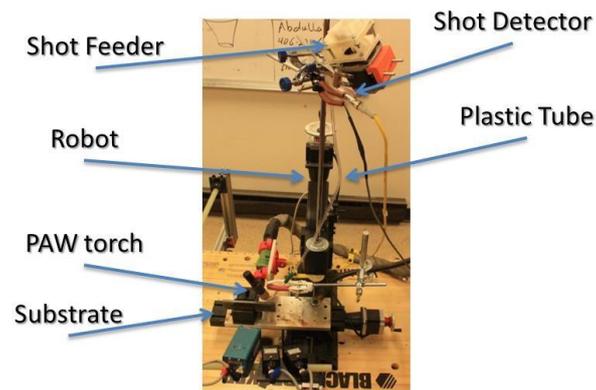
*Figure 2: Experimental setup design with shot feeder*

Deposit walls were built by placing individual weld layers were placed one atop the previous layer (Fig. 3). The time to complete one individual weld layer, $t_t$, is determined from the wall length, $l_t$. The time from the start of one weld layers to the next is the sum of the weld layers deposit time, $t_t$, and the intertrack wait time $t_t$. That is, for a given deposit, the inter-track wait time was proportional to the weld track time via . The inter-track wait time allowed cooling of the deposit between weld tracks.   was the primary experimental means to control deposit temperature, TD, and therefore to control weld track cooling rate and microstructure development.
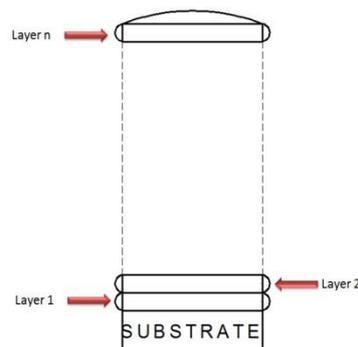


*Figure 3: Idealized weld metal deposit build progression*

## Metallography of Weld Metal Specimen

The waiting time between layers was 1 minute. The PAW essential process parameters used to manufacture the Specimen are shown in Table 1 (Appendix A). Specimen was built using 1018 steel.

The substrate was 150 mm long by 32 mm high and 6.5mm thick. The Specimen was 26 layers producing a deposit 100 mm long by 17 mm high and 7 mm thick. Layer deposition always started from the same end. After each layer, the deposit height was remeasured. The specimen was allowed one minute to cool down between layers.

The deposit grains size change from a relatively small grain size near the substrate to a very coarse microstructure with a large grain size near the tip of the deposit. Figure 4 shows the specimen grains change.

The microstructure of the specimen near the substrate consisted of pearlite colonies (dark contrast) and ferrite grains (light contrast). Both ferrite and pearlite grains were nearly equiaxed grains, ranging from 25 to 50 μm in size.
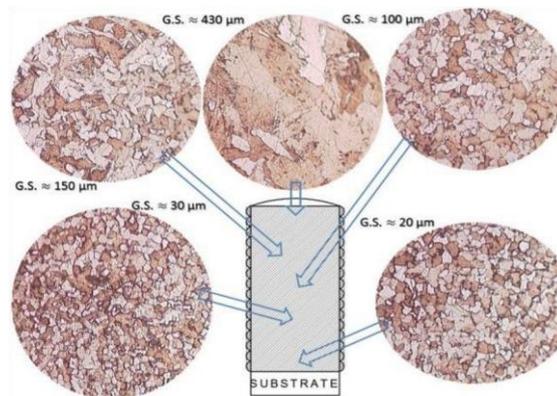


*Figure 4: Transverse macro section of the specimen with example micrographs and grain size at deposit heights*

The microstructure of the specimen near the surface, the light-colored region of the microstructure, is the ferrite. The grain boundaries between the ferrite grains can be seen quite clearly. The dark regions are the pearlite. It is made up from a fine mixture of ferrite and iron carbide, which can be seen as a "wormy" texture. Both ferrite and pearlite grains were columnar grains which are long, thin, coarse grains, ranging from 300 to 430 μm in size.

## Analytical Deposit Model Development

A simple analytical heat flow model, developed (Ref.9) was used to simulate the deposit build temperature $T_{dep}$ in previous work (Ref.10). That model was modified to suit the experimental parameters used in this work. The results of the analytical heat flow model provide the foundation on which to develop a strategy to manage deposit heat flow.

For many heat transfer problems, the first law of thermodynamics provides a useful, often essential tool for heat flow analysis. The conservation of energy for a control volume is given as (Ref.11):

$$\Delta E_{st} = E_{in} - E_{out} + E_g \quad \textbf{Eq1}$$

Since no mechanical work is performed on the control volume, and no energy is generated within the control volume, only thermal energy is considered.
Equation 1 can be rewritten as (Ref.10):

$$Q_{dep} = Q_{weld} - (Q_{cond} + Q_{conv} + Q_{rad}) \quad \textbf{Eq2}$$ Mass, surface area and heat are added to the deposit with each successive weld layer. The model is designed for general methods of layers-based additive manufacturing. A layer can be produced from multiple tracks laid side-by-side as shown in Figure 5 (A) or can be produced from a single track as shown if Figure 5 (B)
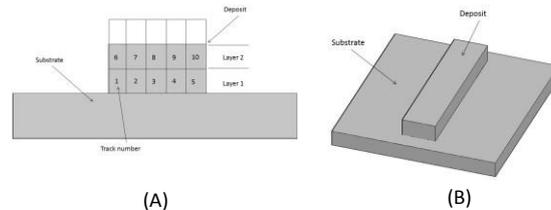
(A)                                        (B)

*Figure 5: (A) shown A layer can be produced from*
*multiple tracks laid side-by-side (B) shown a Layer can be produced from a single track.*

The cumulative weld metal deposit mass increases as the manufacturing of the deposit increases according to (Ref.10):

$$m_{dep} = m_o + \sum_{n_l=1}^{N_l} \left( \sum_{n_t=1}^{N_t} \Delta m_t \right)$$

**Eq3**

The cumulative weld metal deposit area similarly increases as (Ref.10).

$$A_{dep} = A_o + \sum_{n_l=1}^{N_l} \left( \sum_{n_t=1}^{N_t} \Delta A_t \right)$$

**Eq4**

The deposit thermal energy gained via PAW for each weld track is given by:

$$Q_{weld} = \lambda . \eta_{.} E_{avg} . I_{avg} . t_l \qquad \textbf{Eq5}$$

The term λ has physical significance in that it can represent PAW heat transfer efficiency and accounts for heat losses during energy transfer from the arc to the deposit.

In this work, the arc was pulsed from a background level to peak level and back to the background level for each shot delivered to the deposit. Thus each
layer required multiple current pulse cycles such that

$$t_t = n_p \left( t_p + t_B \right) \qquad \textbf{Eq6}$$

To account for arc current pulsing equation 5 is written as

$$Q_{weld} = (I_B . E_B . t_B + I_P . E_p . t_p) . \lambda . n_p \qquad \textbf{Eq7}$$

To simplify the model solution, heat is the considered only to be lost while the arc is off during the interlayer wait-time $\delta t_t$. Heat is lost via radiation according to:

$$Q_{rad} = \psi \sigma \varepsilon A_{dep} (T_{dep}^4 - T_{sur}^4)(\delta t_t) \qquad \textbf{Eq8}$$

The term ψ is the scale factor to modify the magnitude of heat lost from the deposit due to radiation. The term ψ has physical significance and can be used as modification of the surface area of the deposit, and/or variations of ε as deposit temperature changes and/or changes in the temperature of the surroundings.

Heat loss by conduction occurred out the sides and bottom of the substrate into the fixture. Heat is lost via conduction according to:

$$Q_{cond} = \xi h_{cond} A_{contact}(T_{dep} - T_{sur})(\delta t_t) \ \textbf{Eq9}$$

The term $\xi$ has physical significance and can be used as modification of the contact area between the substrate and the fixture, and/or the conduction heat transfer coefficient between the substrate and the fixture, and/or changing the temperature of the fixture in contact with the substrate. Heat lost from the deposit via convection occurs according to (Ref.11):

$$Q_{conv} = \zeta h_{conv} A_{dep}(T_{dep} - T_{\mathrm{sur}})(\delta t_t) \qquad \textbf{Eq10}$$

## Analytical Heat Flow Model Solution

The analytical heat flow model is solved for the deposit temperature, $T_{dep}$, as a function of the number of weld tracks, $n_t$, in the weld metal deposit. The amount of heat accumulated in the weld metal deposit at any instant can be expressed as:

$$Q_{dep} = m_{dep} c_p (T_{dep} - T_{sur}) \qquad \textbf{Eq11}$$

If the right-hand-side of Equation 11 for $Q_{dep}$ is substituted into Equation 2, the result becomes:

$$m_{dep} C_p =$$
$$(T_{dep} - T_{sur}) = \textbf{Eq12}$$
$$Q_{weld} - (Q_{cond} + Q_{conv} + Q_{rad})$$

Solving Equation 12 for Tdep results in:

$$T_{dep} = \frac{Q_{weld} - (Q_{cond} + Q_{conv} + Q_{rad})}{m_{dep} c_p} + T_{sur} \qquad \textbf{Eq13}$$

and by recognizing that $Q_{weld}, Q_{cond}, Q_{conv}, Q_{rad}$, and $m_{dep}$ are functions of time and, therefore, weld track number, $n_t$, the weld metal deposit temperature, $T_{dep}$, can be expressed as:

$$T_{dep}(n_t)$$
$$= \frac{Q_{weld}(t_l) - [Q_{cond}(\delta t_t) + Q_{conv}(\delta t_t) + Q_{rad}(\delta t_t)]}{m_{dep}(n_t)c_p} \qquad \textbf{Eq14}$$
$$+ T_{dep}(n_{t-1})$$

Where

$$t_t = n_p(t_p + t_B) \ \textbf{Eq15}$$

## Analytical Heat Flow Model Assumptions and Solution Approach

Several assumptions are used to simplify the analytical heat flow model. First, the weld metal deposit thermal energy gained via PAW,$Q_{weld}$, enters the deposit and diffuses evenly throughout the substrate and deposit immediately after the layer is completed. The first assumption infers that the deposit thermal conductivity is large, and deposit diffusion distances are small. Another assumption is that no heat is lost via conduction, convection, and radiation during the time it takes to complete a weld track. $Q_{Cond}$,$Q_{conv}$, and $Q_{rad}$only occur during the inter-track wait time, $\delta t_t$. The initial temperature of the substrate and of the fixture that the substrate rests upon is assumed to be the ambient temperature environment ($T_{sur}$), (Ref.10).

The approach taken to solve the analytical heat flow model on a track-by-track basis is described as follows. $Q_{weld}$ and $\Delta m_t$ are added to the deposit. As a result of the newly added mass and heat, an intermediate weld metal deposit surface temperature, Ti, is calculated. $\Delta A_t$ is added to the deposit, and $Q_{Cond}$ $Q_{,conv}$, and $Q_{rad}$are removed from the deposit at the intermediate. As a result of the newly lost heat, the deposit temperature, $T_{dep}$, is calculated and becomes the starting deposit temperature for the next weld track. Iterations continue for the specified number of weld metal deposit layers.

## Results and Discussion of the Analytical
### Heat Flow Model

 The result of the analytical heat flow model is $T_{dep}$ as a function of $t_t$ $n_t$, $\lambda$, $\psi$, $\xi$, and $\zeta$. The coefficients $\lambda$, $\psi$, $\xi$, and $\zeta$ were adjusted to allow the analytical heat flow model deposit temperature to approximate the experimental measured deposit temperature. two $\delta t_t$values were used, the actual specimen was $\delta t_t 1min$ = 60 sec and hypothetical value of $\delta t_t$= 10 sec. The model is capable of predicting  $T_{dep}$ (nt) for an unlimited number of layers, however in this research, $n_t$ was limited to be 200 layers. The analytical heat flow model was solved by using a spreadsheet computer program. Analytical heat flow model properties for low-carbon steel, along with their typical values, are also shown in (Ref.15). The analytical heat flow model properties and mathematical formulas were taken from Refs.
(Ref.12), (Ref.13) and (Ref.14).

 Deposit mass, surface area and heat input increase linearly with$n_t$. Increased mass causes the deposit to contain more thermal energy, while increased surface area allows the deposit to shed more thermal energy via radiation and convection. Increased deposit height reduced the amount of heat loss to the fixture via conduction. A maximum $T_{dep}$ was selected for a steel deposit based on the Fe-C phase diagram. Ideally, $T_{dep}$ would stay below the eutectoid temperature  approximately  2     Lower temperature reduces grain growth and produces a refined microstructure in the deposit, both of which lead to better mechanical properties.

As mentioned the scale factors, $\lambda$, $\psi$, $\xi$, and $\zeta$ were adjusted to match the model simulated deposit temperature to the experimental deposit temperature. Figure 6 shows experimental and simulation $T_{dep}$ as a function of $n_t$. The experimental deposit temperature measurements are shown in Tables 25 and 26 the values for the model scale factors $\lambda$, $\psi$, $\xi$, and $\zeta$ used in Figure 6
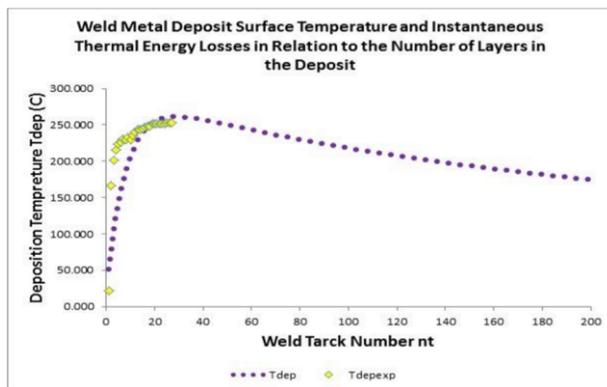
*Figure 6: Experimental and Simulation         as a function of nt*

Since the model shows very close results from the beginning of the building to 26 layers, a prediction can be made from the graph. For this solution to the analytical heat flow model, $\delta t_t$ = 1 minute (60 seconds), which is the same $\delta t_t$ that was used to manufacture the specimen. Other property values used to solve the analytical heat flow model are shown in (Ref.15). The values of $\lambda$, $\xi$, $\psi$, and $\zeta$, are listed in Table 2.This allows the model temperatures to predict the approximation of the experimental temperatures. Since the model shows very close results from the beginning of the building to 26 layers, a prediction can be made from the graph

The model was tuned using the perimeter reasonably match the experimental deposit temperature. In Figure 7, the total number of experimental temperature reading results is limited to the experimental range of layers ( $\approx$ 26).With the values of $\delta$ (0.28) $T_{dep}$ increases to a peak value of approximately 200 °C after 26 layers. $T_{dep}$ begins to decrease slightly after each individual layer as predicted by the model.

The conditions used to obtain the solution to the analytical heat flow model for the specimen shown in Figure 6 represent a condition of high heat loss via conduction. Conduction is the dominant heat loss mechanism for the prescribed conditions, as the number of layer increases the heat loss via conduction decrease. The amount
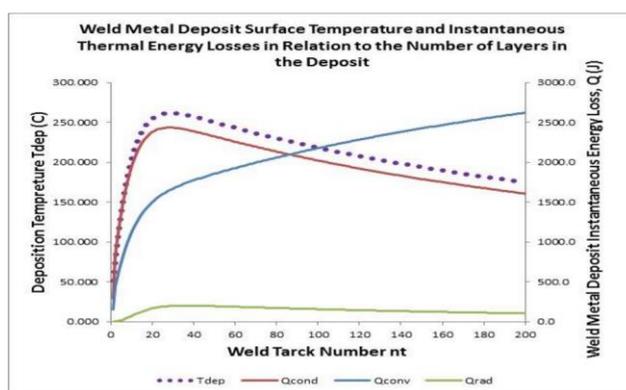


*Figure 7: Experimental and Simulation         as a function of nt for $\delta tt$ = 60 seconds*

of heat loss by conduction is depending on the temperature deposited and the distance of the heat have to travel through the specimen to the fixture is linear with deposit height and deposit temperature. As the height of the deposit increases the heat loss by conduction decreases, for two reasons; the temperature of the deposit decreases and the height of the deposit increase.

An increased in heat lost via convection to be the dominate heat loss with increase in number of layers. Convection accounts for most thermal energy losses as the area increases. The curve of the heat loss via convection can be understood better with referral to equation (10). Heat loss via radiation is the lower heat loss, although increase in area is a direct factor to increase in heat loss via radiation. However, the reduction in temperature deposited has more effect since the temperature in $Q_{rad}$ is raised to the power 4 (see equation 8). All of the heat transfer mechanisms increase with increasing $n_l$ to a certain level and approach a maximum value, and then start to decrease except convection as a result of the increasing $A_{dep}$.

$T_{dep}$ generally increases as more weld metal layers are deposited when $n_l$ is small. When $n_l$ is small, $T_{dep}$ increases linearly. As more weld layers are deposited, the rate at which $T_{dep}$ increases begins to decrease. After certain $A_{dep}$ is reached, $T_{dep}$ reaches a maximum value and begins to decrease as a result of the combined effects of thermal energy losses resulting from conduction, convection, and radiation. The values used to develop Figure 8 are displayed in Table 2 (located in Appendix A).

The analytical heat flow model shown in Figure 8 demonstrated that higher maximum values of $T_{dep}$ can be achieved by decreasing $\delta t_t$ to 10 second. This is a relatively small value of $\delta t_t$, which is effective at increasing productivity. Productivity can be boost at the expense of mechanical properties. A plot of the simulation $T_{dep}$ developed from the analytical heat flow model for $n_t = 200$ is shown in Figure 7.
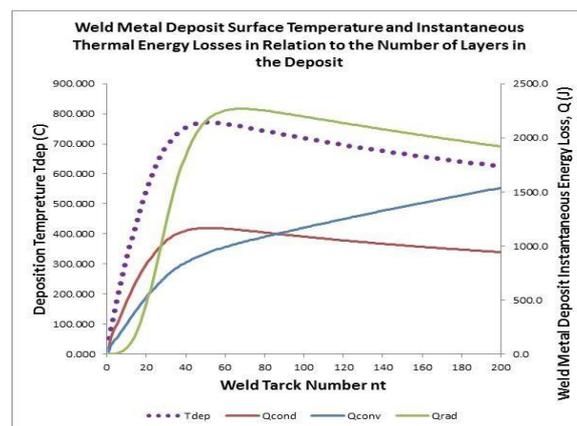


*Figure 8: Experimental and Simulation $T_{dep}$ as a function of nt for δtt = 10 seconds*

The wait time was decrease more than 6 times from the calibrated model. The heat transfer mechanisms did not behave the same as $\delta t_t = 1$ minute (60 Sec.). The conditions used to obtain the solution to the analytical heat flow model for shorter inter-layer wait-time in Figure 8 represent a condition of high heat loss via Radiation. The increase in temperature deposited has direct effect in $Q_{rad}$ since the temperature in $Q_{rad}$ is raised to the power 4 (see equation 8). Conduction also, increases to a peak level then as the number of layer increases the heat loss via conduction decrease. Thermal energy loss via convection increase linearly as the area increases.

$T_{dep}$ is greater comparing to $\delta t_t = 1$ minute (60 Sec.). Generally, increases as more weld metal layers are deposited when $n_l$ is small. When $n_l$ is small, $T_{dep}$ increases. As more weld layers are deposited, the rate at which $T_{dep}$ begins to decrease linearly. After certain $A_{dep}$ is reached, $T_{dep}$ reaches a maximum value and begins to decrease as a result of the combined effects of thermal energy losses resulting from conduction, convection, and radiation. The values used to develop Figure 8 are displayed in Table 2 (located in Appendix A).

Higher values of $T_{dep}$ increase grain growth and produce columnar grains which are long, thin, coarse grains microstructure in the deposit. Poorer mechanical properties are achieved as a result of increase in grain growth and coarse microstructures in the weld metal deposit. $T_{dep}$ reaches the mild steel eutectoid temperature in the Fe-C phase diagram (about 727 C) which will lead to eutectoid transformation to produce ferrite and cementite. The possibility of improving thermal energy flow from the weld metal deposit is demonstrated by the analytical heat flow model. Improving heat flow from the deposit controls the weld metal microstructure while simultaneously maintaining high productivity. An important step in the advancement of AM techniques is thermal management of the weld metal deposit. Thermal management of the weld metal deposit controls the deposit temperature and, therefore, microstructure development and the resulting mechanical properties (Ref.10).

## Conclusion

An analytical heat flow model was developed to study the influence of interlayer wait time on deposit temperature and therefore grain size and hardness. The results of the model indicated that as wall height increased, the rate of deposit heat removal by conduction to the substrate decreased leading to a higher preheat temperature after a fixed interlayer wait time causing grain size to increase as wall height increased.

The model results also show that as wall height increased, the deposit surface area from which heat energy is lost via convection and radiation increased. The model also demonstrated that the use of a means of forced convection to rapidly remove heat from the deposit could be an effective way to boost productivity and maintain smaller grain size and therefore higher hardness and strength in the deposit.

## Acknowledgments

## References

1. **C.O. Brown, E.M. Breinan and B.H. Kear.** *Method for Fabricating Articles by Sequential Layer Deposition. 4.323.756* U.S. , 1982.

2. **Edmonds, M.D. McAninch and D.P.** *Method and Apparatus for Building a Workpiece by Deposit Welding. 4,775,092.* U.S., 1988.

3. *Electron Beam Freeform Fabrication Fabrication:*
*A Metal Deposition Apparatus to Build Components*
*Directly from CAD.* **Taminger, Karen.** Arlington,
Texas : NASA Langley Research Center, March 26-
27, 2008. available at technologygateway.nasa.gov/docs/EBF3Overview.pdf.

4. *Electron Beam Freeform Fabrication for Cost*
*Effective Near-Net Shape Manufacturing.* **Hafley,**
**Karen M. Taminger and Robert A.** s.l. : NASA
Langley Research Center. Metals & Thermal

Structures Branch. Mail Stop 188A, Hampton, VA 23681-2199 USA available at technologygateway.nasa.gov/docs/20080013538_200 8013396.pdf.

5. *Direct Digital Manufacturing of Metallic*

*Components: Direct Digital Manufacturing of*

*Metallic Components Affordable, Durable, and*

*Structurally Efficient Airframes.* **Frazier, W.E.** at the Holiday Inn, Solomons Island, MD : s.n., 11 - 12 May 2010, Vision and Roadmap.

6. Sciaky Manufacturing. [Online] http://www.sciaky.com/direct_manufacturing.html.

7. *Qualification of Metallic Materials and Structures for Aerospace Applications.* **William Frazier, Don Polakovics, and Wayne Koegel.** March 2001, JOM.

8. *Shaped Metal Deposition of a Nickel Alloy for Aero Engine Applications.* **Clark, D., M. R. Bache, and M. T. Whittaker.** 2008, Journal of Materials Processing Technology 203, pp. 439-448.

9. **Stavinoha, Joe N.** *Investigation Of Plasma Arc Welding As A Method For The Additive Manufacturing Of Ti-6Al-4V Alloy Components.* Butte : Montana Tech, 2012.

10. *Measurement And Simulation Of Titanium Alloy*

*Deposit Temperature In Electron Beam Additive*

*Manufacturing.* **Madigan, R. Bruce, Sean F. Riley, Mark J. Cola, Vivek R. Dave, and John E.**

**Talkington.** Chicago, Illinois : ASM International,, 2012. Ninth International Trends in Welding Research Conference.

**11. Incropera, Frank P., David P. DeWitt, Theodore L. Bergman, and Adrienne S. Lavine.**

*Introduction to Heat Transfer.* Fifth ed. Hoboken. New Jersey : John Wiley & Sons, Inc., 2007.

**12. Donachie, Matthew J.** *Titanium Technical Guide.* Second. Materials Park, Ohio : ASM International, 2000.

**13. Messler, Robert W.** *Principles Of Welding:*

*Processes, Physics, Chemistry, And Metallurgy.* s.l. : Weinheim, Baden-Württemberg, Germany: WileyVCH., 2004.

**14. Association, Staff of Research and Education.** *The Handbook of Mechanical Engineering.* Piscataway, New Jersey : Research and Education Association., 2004.

**15. Alhuzaim, Abdullah F.** *INVESTIGATION IN THE USE OF PLASMA ARC WELDING AND*

*ALTERNATIVE FEEDSTOCK DELIVERY METHOD IN ADDITIVE MANUFACTURE.* Butte, MT :

Montana Tech of the university of Montana, 2014. Available at

http://www.abdullahalhuzaim.com/wpcontent/uploads/2014/05/Additive-Manufacture.pdf

**Appendix A**

**Table 1: Essential Variables for PAW**

| Parameter | Value/Range |
|---|---|
| Automation Level | Mechanized/Robotic |
| Electrode Setback | Gauge 1 |
| Orifice Diameter | 2.4mm |
| Shielding Gas | Argon @ 18CFH |
| Plasma Gas | Argon @ 2CFH |
| Voltage | Vp = 20V Vb =16V |
| Amperage | Ip = 50A Ib = 9A |

| Current Type | DCEN |
|---|---|
| Tungsten Type/Size/Prep | W+Th,La,Cs / 2.4mm / Pointed with landing |
| Travel Speed | Actual 22.22mm/min  Theoretical 20mm/min |
| Torch Stand-off | 4mm |
| Filler Material | 1018 Steel |
| Base Material Substrate | A36 Steel |
| Transfer Mode | Transferred Arc |
| Welding Mode | Melt-In |

**Table 2: Properties Used to Solve the Analytical Heat Flow Model**

| Model Property | Value1 |
|---|---|
| mo (g) | 2607.400000 |
| $\Delta mt$  g | 3.280500 |
| Ao (m2) | 0.011966 |
| $\Delta At$  m2 | -04 |
| cp [J/(g·°C)] | |
| $\varepsilon$ | 1.280000E |
| | 0.050000 |
| | 0.500000 |
| $\zeta$ [W/ m2·K4 ] | 5.670000E-08 |
| Qweld (J) | 11880.0 |
| $\delta tt$ (s) | 60 |
| | 50 |
| | 13 |
| | |
| hcond [W/(m2·K)] | |
| hconv [W/(m2·K)] | |
| $\lambda$ | 0.60 |
| $\xi$ | 0.50 |
| $\zeta$ | 0.50 |
| $\psi$ | 1.00 |
| Tsur (°C) | 22.00 |

**Appendix B**
**Glossary of Terms**  Term Definition

| Term | Definition |
|---|---|
| A | Ampere |
| *Aarc* | Arc area (mm2) |
| AC | Alternating current |
| *Adep* | Cumulative deposit area (in².) |
| Ain | Inner surface area of deposit (in².) |
| AM | Additive manufacturing |
| *Ao* | Original substrate area (in².) |
| A36 | Plain carbon steel alloy |
| CAD | Computer-aided design |
| Cb | Columbium |
| CC | Constant current |
| DC | Direct current |
| DCEN | Direct current electrode negative |
| DM | Direct manufacturing |
| *Eg* | Thermal energy generation in a control volume (J) |
| *Ein* | Thermal and mechanical energy entering a control volume (J) |
| *Eout* | Thermal and mechanical energy leaving a control volume (J) |
| FFF | Free-form fabrication |
| HAZ | Heat-affected zone |
| *hcond* | Conduction heat transfer coefficient [$W/m2 \cdot K$] |
| *hconv* | Convection heat transfer coefficient [$W/m2 \cdot K$] |
| hcp | Hexagonal close-packed |
| *hspec1* | Specimen 1 height (mm.) |
| *hspec2* | Specimen 2 height (mm.) |
| *ht* | Weld track height (mm.) |
| *Iarc* | Arc current (A) |
| In. | Inch |
| J | Joule |
| K | Kelvin |
| kg | Kilogram |
| ksi | 1,000 pounds per square inch |
| lb. | Pound |
| LM | Layered manufacturing |
| m | Meter |
| MD | Metal deposition |
| *mdep* | Cumulative deposit mass (kg) |
| min | Minute |
| mm | Millimeter |
| *mo* | Original substrate mass (kg) |
| *nl* | Layer "n" in the deposit |
| *Nl* | Number of layers per deposit |
| *nt* | Track "n" in the deposit |

| | |
|---|---|
| *Nt* | Number of tracks per layer |
| *Parc* | Arc power (*W*) |
| PAW | Plasma arc welding |
| *PD* | Power density (*W*/mm2) |
| psi | Pounds per square inch |
| *Q* | Deposit thermal energy lost (J) |
| *Qcond* | Deposit thermal energy lost via conduction (J) |
| *Qconv* | Deposit thermal energy lost via convection (J) |
| *Qdep* | Accumulated deposit thermal energy (J) |
| *Qrad* | Deposit thermal energy lost via radiation (J) |
| *Qweld* | Deposit thermal energy gained via PAW (J) |
| RM | Rapid manufacturing |
| RP | Rapid prototyping |
| s | Second |
| sl | Substrate length (mm.) |
| sw | Substrate width (mm.) |
| sh | Substrate height (mm.) |
| SMD | Shaped metal deposition |
| sv | Substrate volume (mm³) |
| *Tdep* | Deposit temperature (°C) |
| Texp | Experimental deposit surface temperature (°C) |
| Tfluid | Fluid temperature (°C) (used in Mathcad analytical heat flow model solution) |
| To | Original deposit surface temperature (°C) |
| Ts | Deposit temperature (°C) (used in Mathcad analytical heat flow model solution) |
| tspec | Specimen thickness (mm.) |
| *Tsur* | Surrounding/ambient temperature (°C) |
| *tt* | Time to weld one track (s) |
| *V* | Voltage |
| W | Tungsten |
| *W* | Watt |
| wt% | Weight percent |
| *δtt* | Wait time between weld tracks (min) |
| Δ*At* | Area added to substrate after each weld track (mm.2) |
| Δ*Est* | Change in thermal and mechanical energy stored in a control volume (J) |
| Δ*mt* | Mass added to substrate after each weld track (kg) |
| *ε* | Emissivity |
| *ζ* | Scale factor to modify the convection heat transfer coefficient |
| *ζhconv* | Modified effective convection heat transfer coefficient [*W*/ m2·K ] |
| *λ* | Scale factor to modify the PAW heat transfer efficiency |
| *η* | Modified effective PAW heat transfer efficiency (%) |
| μm | Micrometer (1 x 10-6 m) |
| *ξ* | Scale factor to modify the conduction heat transfer coefficient |
| *ξhcond* | Modified effective conduction heat transfer coefficient [*W*/ m2·K ] |
| *π* | Mathematical constant ≈ 3.14 |

| | |
|---|---|
| $\rho$ | Density (g/cm3) |
| $\zeta$ | Stefan-Boltzmann constant [5.67 x 10-8 *W*/ m2·K4 ] |
| $\Sigma$ | Summation |
| $\psi$ | Scale factor to modify the magnitude of heat lost due to radiation |
| $\zeta$ | Modified effective Stefan-Boltzmann constant [*W*/ m2·K4 ] |